


Article

Quantum State of the Fermionic Carriers in a Transport Channel Connecting Particle Reservoirs

Andrey R. Kolovsky^{1,2,*}  and Dmitrii N. Maksimov^{1,2,3}

¹ L.V. Kirensky Institute of Physics, Federal Research Center KSC SB RAS, 660036 Krasnoyarsk, Russia; mdn@tnp.krasn.ru

² Department of Engineering Physics and Radio Electronics, Siberian Federal University, 660041 Krasnoyarsk, Russia

³ Department of Space Technologies and Materials, M.F. Reshetnev Siberian State University of Science and Technology, 660037 Krasnoyarsk, Russia

* Correspondence: andrey.r.kolovsky@gmail.com

Received: 16 September 2019; Accepted: 14 October 2019; Published: 15 October 2019



Abstract: We analyze the quantum state of fermionic carriers in a transport channel attached to a particle reservoir. The analysis is done from first principles by considering microscopic models of the reservoir and transport channel. In the case of infinite effective temperature of the reservoir we demonstrate a full agreement between the results of straightforward numerical simulations of the system dynamics and the solution of the master equation on the single-particle density matrix of the carriers in the channel. This allows us to predict the quantum state of carriers in the case where the transport channel connects two reservoirs with different chemical potentials.

Keywords: quantum transport

1. Introduction

Electron transport in mesoscopic devices is a wide subfield in solid-state physics [1–3]. The studies on electron transport are aimed at control of the electron current between two or more contacts (electron reservoirs) attached to a quantum device. Recently, the problems of the same kind have been addressed for the principally different system—charge neutral atoms in laser-based devices, both experimentally [4–7], and theoretically [8–22]. The advantage of the latter systems against the electron system is the perfect control over the system parameters and effective detection techniques that allow for in situ measurement of the quantum state of carriers in the device which, following Reference [4], we refer to as the transport channel connecting particle reservoirs.

On the formal level the quantum state of carriers in the transport channel is characterized by the single-particle density matrix (SPDM), the knowledge of which suffices to predict the current between reservoirs. In the present paper we analyze the SPDM of fermionic carriers from first principles with the emphasis on decoherence effect of reservoirs. Clearly, to address this problem from first principles one needs physically relevant microscopic models of the transport channel and particle reservoir. Having in mind cold atoms we model the transport channel by the tight-binding chain, which is known to adequately describe neutral atoms in deep optical lattices. (Here ‘deep’ means that the width of the ground Bloch band is smaller than the energy gap separating it from the rest of the spectrum.) As for the particle reservoir, we model it by the Two-Body Random Interaction Model (TBRIM) [23,24] that corresponds to a system of N weakly interacting spinless fermions distributed over M natural orbitals. The closed (isolated) TBRIM possesses the self-thermalization property [25,26]. This means, in particular, that one has a meaningful notion of the temperature of TBRIM, despite the fact that the system has no contact with a thermostat. It has been also shown in the recent work [27] that TBRIM

retains the self-thermalization property when the system is open, which makes it an excellent model for the reservoir of fermionic particles.

The structure of the paper is as follows. After reviewing TBRIM in Section 2, we attach a finite-length tight-binding chain to this reservoir and study particles propagation across the chain in Section 3. We quantify decoherence effect of the reservoir on the carriers in the channel by the von Neumann entropy of SPDM and show that it is strictly positive. In Section 4 we compare the exact numerical results with those obtained by using the master equation on the reduced density matrix of the carriers (RDM). Finally, in the concluding Section 5 we summarise the results and give the list of open problems.

2. The Model

In this section we specify the system Hamiltonian \hat{H} , which consists of the Hamiltonian of the particle reservoir \hat{H}_b , the Hamiltonian of the transport channel \hat{H}_s , and the coupling Hamiltonian \hat{H}_{int} :

$$\hat{H} = \hat{H}_b + \hat{H}_s + \hat{H}_{int} . \tag{1}$$

2.1. The Particle Reservoir

We model the particle reservoir by TBRIM which describes N interacting spinless fermions distributed over M natural orbitals with the energies ϵ_k ($\epsilon_{k+1} \geq \epsilon_k$):

$$\hat{H}_b = \sum_{k=1}^M \epsilon_k \hat{d}_k^\dagger \hat{d}_k + \epsilon_b \sum_{ijkl} V_{ij,kl} \hat{d}_i^\dagger \hat{d}_j^\dagger \hat{d}_k \hat{d}_l . \tag{2}$$

Here operators $\hat{d}_i^\dagger, \hat{d}_i$ satisfy the usual anti-commutation relation and one-particle energies ϵ_k and interaction constants $V_{ij,kl}$ are random (up to the obvious symmetry relations insuring hermiticity of the Hamiltonian) variables with standard deviation equal to unity. The parameter ϵ_b in the Hamiltonian (2) controls the strength of two-body interactions which couples every Fock state with other $K = 1 + N(M - N) + N(N - 1)(M - N)(M - N - 1)/4$ Fock states. In the paper we assume $\epsilon_b \ll 1$, i.e., we consider the limit of weakly interacting fermions. Yet, ϵ_b must larger than the critical value where TBRIM shows the transition to Quantum Chaos [28,29]. An analytical estimate for the critical interaction strength can be obtained by using the Åberg criteria [30], while numerically this transition is detected as the change of the level-spacing distribution from the Poisson distribution to the Wigner-Dyson distribution. In what follows we fix the reservoir size to $M = 12, N = 6$, and set $\epsilon_b = 0.0085$ where the energy level statistics perfectly follows the Wigner-Dyson distribution. The chosen ϵ_b is approximately twice larger than the critical value. At the same time, it is small enough to speak of weakly-interacting fermions. In particular, the mean density of states, which in the case of non-interacting fermions is well approximated by the Gaussian of the width $\sim \sqrt{N}$, remains practically unaffected.

Provided the condition of Quantum Chaos is satisfied, the system (2) shows the phenomenon of self-thermalization [26]. It means that for any given eigenstate $|\psi_E\rangle$ occupation numbers of the natural orbitals $n_k = \langle \psi_E | \hat{d}_k^\dagger \hat{d}_k | \psi_E \rangle$ obey (of course, with some fluctuations) the Fermi-Dirac distribution,

$$n_k = \frac{1}{e^{\beta(\epsilon_k - \mu)} + 1} , \tag{3}$$

where the inverse effective temperature β and the chemical potential μ are uniquely determined by the eigenstate energy E and the number of particles N through the solution of the following system of two non-linear algebraic equations,

$$\sum_{k=1}^M \frac{1}{e^{\beta(\epsilon_k - \mu)} + 1} = N , \quad \sum_{k=1}^M \frac{\epsilon_k}{e^{\beta(\epsilon_k - \mu)} + 1} = E . \tag{4}$$

Then the ground and the highest energy eigenstates of the system (2) corresponds to $\beta = \pm\infty$, while an eigenstate from the middle of the spectrum corresponds to $\beta = 0$. We mention that Equations (3)–(4) also hold for the open TBRIM [27], where the number of particles changes in time.

2.2. The Transport Channel

We model the transport channel by the tight-binding chain,

$$\hat{H}_s = V_g \sum_{l=1}^L \hat{c}_l^\dagger \hat{c}_l - \frac{J}{2} \left(\sum_{l=1}^{L-1} \hat{c}_{l+1}^\dagger \hat{c}_l + h.c. \right), \quad (5)$$

where J is the hopping matrix element and V_g has the meaning of the gate voltage. We shall characterise fermions in the channel by SPDM,

$$\rho_{l,m}(t) = \langle \Psi(t) | \hat{c}_l^\dagger \hat{c}_m | \Psi(t) \rangle, \quad (6)$$

where $|\Psi(t)\rangle$ is the total wave function of the whole system defined in the Hilbert space of the dimension

$$\mathcal{N} = \frac{(M+L)!}{N!(M+L-N)!}. \quad (7)$$

Since the quadratic form $\hat{c}_l^\dagger \hat{c}_m$ in Equation (6) conserves the number of particles, the density matrix (6) can be presented as a sum of partial density matrices,

$$\rho(t) = \sum_{i=1}^L \rho^{(i)}(t), \quad (8)$$

where $\rho^{(i)}(t)$ refer to the fixed number fermions in the channel. We note that for an isolated channel with i fermions in a pure state the matrix $\rho^{(i)}(t)$ has i eigenvalues equal to unity and $L - i$ eigenstates equal to zero.

2.3. The Coupling Hamiltonian

Particles from the reservoir enter the transport channel due to the coupling controlled by the Hamiltonian

$$\hat{H}_{int} = \varepsilon \left(\sum_{k=1}^M W_k \hat{c}_1^\dagger \hat{d}_k + h.c. \right), \quad (9)$$

where W_k are random entries of the same magnitude as the interaction constants $V_{ij,kl}$ and ε is our control parameter. In what follows we consider the situation where initially all particles are in the reservoir, i.e.,

$$|\Psi(t=0)\rangle = |\psi_E\rangle \otimes |vac\rangle. \quad (10)$$

3. System Dynamics

In this section we discuss the system dynamics governed by the Schrödinger equation with the Hamiltonian (1) for the initial condition specified in Equation (10).

3.1. Population Dynamics

Figure 1 shows the occupation numbers of the natural orbitals and the chain sites,

$$\begin{aligned} n_k(t) &= |\langle \Psi(t) | \hat{d}_k^\dagger \hat{d}_k | \Psi(t) \rangle|^2, \\ n_l(t) &= |\langle \Psi(t) | \hat{c}_l^\dagger \hat{c}_l | \Psi(t) \rangle|^2, \end{aligned} \quad (11)$$

as the function of time for $|\psi_E\rangle$ from the middle of the spectrum of the system (2) where all reservoir modes are equally populated, i.e., $n_k \approx N/M$. According to Equation (3) this corresponds to the infinite temperature of the reservoir. One distinguishes two qualitatively different stages/regimes in Figure 1. During the first stage fermionic particles propagate in the channel with the velocity determined by the hopping matrix element J in Equation (5). Reaching the boundary particles are reflected back towards the reservoir. Notice that during this stage, which we refer to as propagation stage, the number of particles in the channel monotonically increases. During the second stage, which we refer to as equilibration stage, occupation of the chain sites and natural orbitals equilibrate at $n_k = n_l = N/(M + L)$.

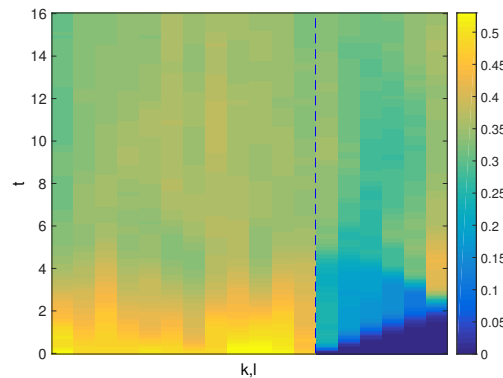


Figure 1. Population dynamics of the reservoir orbitals (left to the vertical dashed line) and the lattice sites (right to the dashed line) for infinite effective temperature of the reservoir. The system size is $M = 12, L = 6$, and $N = 6$. The value of the hopping matrix element $J = 0.5$, the coupling constant $\varepsilon = 0.1$.

To get a deeper insight into the population dynamics we calculate the partial density matrices $\rho^{(i)}(t)$, see Equation (8). The upper panel in Figure 2 shows probabilities $P_i(t)$ to find i fermions in the channel at a given time t , which is given by the equation

$$P_i(t) = \text{Tr}[\rho^{(i)}(t)]/i. \tag{12}$$

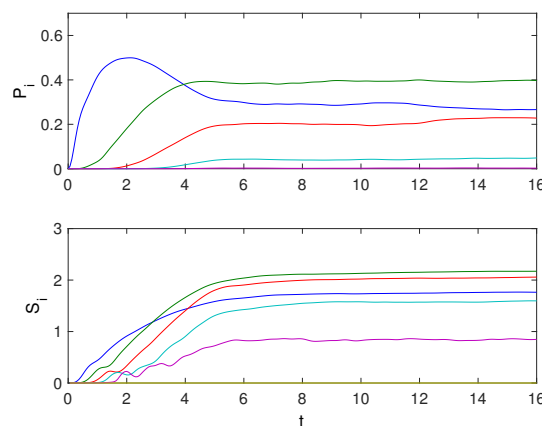


Figure 2. Probabilities P_i to find i fermions in the transport channel (upper panel) and von Neumann entropies S_i of the normalized partial single-particle density matrices (SPDMs) (lower panel) as the functions of time. The different curves correspond to $i = 1$ (blue), 2 (green), 3 (red), 4 (light blue), and 5 (magenta). Probability to find 6 fermions is close to zero and is not shown, as well as the probability to find 0 fermions, which is given by the equation $P_0 = 1 - \sum_{i=1}^L P_i$.

Increasing the evolution time we find $P_i(t)$ to approach the value $P_i(t = \infty) = \mathcal{N}_i/\mathcal{N}$ where \mathcal{N}_i is dimension of the sub-space of the Hilbert space defined by the condition that there are i particles in

the channel. This result proves that for infinite reservoir temperature we have complete equilibration between the system (the tight-binding chain) and the bath (TBRIM).

3.2. Decoherence Dynamics

Next we discuss decoherence effect due to the reservoir. We characterize coherence of the carriers in the transport channel by the von Neumann entropy for the normalised partial SPDMs

$$\rho^{(i)}(t) \rightarrow \frac{\rho^{(i)}(t)}{P_i(t)}, \quad S_i(t) = -\text{Tr}[\rho^{(i)}(t) \log \rho^{(i)}(t)]. \quad (13)$$

(The information von Neumann entropy should not be mismatch with the thermodynamic entropy given by the logarithm of the number of states.) Entropies $S_i(t)$ are depicted in the lower panel in Figure 2. It is seen that decoherence takes place immediately after the particles enter the transport channel and $S_i(t)$ quietly reach the maximally possible values $\bar{S}_i = -i \log(i/L)$ that corresponds to a diagonal matrix with equal matrix elements. The existence of this upper boundary is the main reason for considering the partial SPDMs, which refer to the fixed number of particles, instead of the total SPDM. In fact, the von Neumann entropy $S(t) = -\text{Tr}[\rho(t) \log \rho(t)]$ of the total SPDM Equation (5) depends on the mean number of particles in the chain and, thus, an increase of $S(t)$ does not necessarily indicate decoherence.

A direct consequence of the observed complete decoherence is an irreversible decay of the mean current $j(t)$,

$$j(t) = \text{Tr}[\hat{j}\rho(t)], \quad j_{l,m} = j_0 \frac{\delta_{l,m-1} - \delta_{l-1,m}}{2i}, \quad (14)$$

see red solid line in Figure 3a. We also mention that decay of the mean current is insensitive (at least, on the qualitative level) to variation of the gate voltage V_g , see blue dashed and dash-dotted lines in Figure 3a which correspond to $V_g = \pm 0.5$. This is in a strong contrast with the low-temperature limit, where population dynamics and the mean current crucially depend on inequality relation between the gate voltage and the Fermi energy ϵ_F which is located at $\epsilon = 0$ in the considered case of half-filling $N = M/2$. Indeed, in terms of the reservoir eigenstates the low-temperature limit corresponds to $|\psi_E\rangle$ close to the ground state, where occupation numbers n_k of the natural orbitals show a pronounced step at ϵ_F . Thus, fermions cannot enter the channel if $V_g > J$, where the whole conductance band lies above the Fermi energy. The results of numerical simulation of the low-temperature limit fully confirm this conjecture, see Figure 3b. Let us also notice the enhanced residual fluctuations of the current as compared to the high-temperature limit.

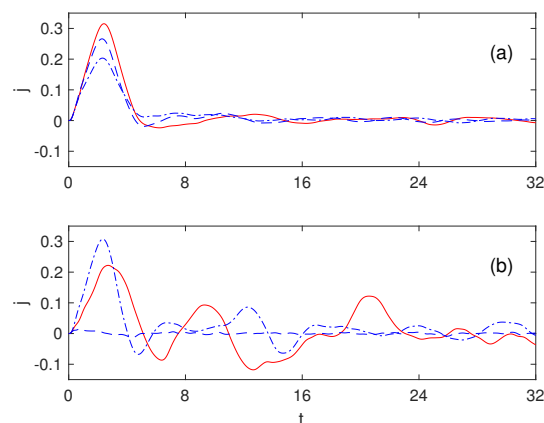


Figure 3. The total current in the transport channel as the function of time in the high-temperature (a) and low-temperature (b) limits. The dash-dotted, solid, and dashed lines correspond to different values of the gate voltage $V_g = -0.5, 0, 0.5$, respectively.

4. Master Equation Approach

It is interesting to compare the results of Section 3 with solution of the master equation on the reduced density matrix $\mathcal{R}(t) = \text{Tr}_b[|\Psi(t)\rangle\langle\Psi(t)|]$ for fermionic carriers in the transport channel. Usually, one considers the following equation:

$$\begin{aligned} \frac{d\mathcal{R}}{dt} &= -i[\widehat{H}_s, \mathcal{R}] - \mathcal{L}_{gain}(\mathcal{R}) - \mathcal{L}_{loss}(\mathcal{R}), \\ \mathcal{L}_{loss}(\mathcal{R}) &= \frac{\gamma}{2}(1 - \bar{n})(\hat{c}_1^\dagger \hat{c}_1 \mathcal{R} - 2\hat{c}_1 \mathcal{R} \hat{c}_1^\dagger + \mathcal{R} \hat{c}_1^\dagger \hat{c}_1), \\ \mathcal{L}_{gain}(\mathcal{R}) &= \frac{\gamma}{2}\bar{n}(\hat{c}_1 \hat{c}_1^\dagger \mathcal{R} - 2\hat{c}_1^\dagger \mathcal{R} \hat{c}_1 + \mathcal{R} \hat{c}_1 \hat{c}_1^\dagger), \end{aligned} \tag{15}$$

where \bar{n} is the filling factor of the reservoir and $\gamma \sim \varepsilon^2$ is the relaxation constant. (This equation also captures the case of bosonic carries, where the prefactor $(1 - \bar{n})$ in the Lindblad term \mathcal{L}_{loss} should be replaced with $(1 + \bar{n})$ and fermionic annihilation and creation operators with bosonic operators.) It should be stressed that the standard derivation of the displayed master equation assumes a number of approximations [31,32], which have to be verified [33,34]. In this sense Equation (15) implicitly refers to the high-temperature limit and is not valid in the low-temperature limit where, as it was demonstrated in the previous section, the system dynamics depends on inequality relation between the Fermi energy and the gate voltage. Also notice that Equation (15) does not involve ε_F as a parameter. For this reason from now on we focus on the high-temperature limit where all required assumptions/approximations are believed to be justified.

4.1. Populations and Decoherence Dynamics

It is easy to prove that the matrix \mathcal{R} in Equation (15) has the block structure where each block is associated with the fixed number of fermions in the tight-binding chain of the length L . Using these blocks we calculate the partial SPDMS,

$$\rho_{l,m}^{(i)}(t) = \text{Tr}[\mathcal{R}^{(i)}(t)\hat{c}_l^\dagger \hat{c}_m], \tag{16}$$

and then use them to calculate probabilities $P_i(t)$ to find i fermions in the transport channel and von Neumann entropies $S_i(t)$, which characterize quantum state of these fermions. The results are presented in Figure 4, which should be compared with Figure 2. We notice that, when solving Equation (15), we take into account depletion of the reservoir, i.e., the parameter \bar{n} is decreased in time according to the depletion dynamics,

$$\bar{n}(t) = (N - N_s(t)) / M. \tag{17}$$

with this minor modification one finds very good agreement between the master equation approach and the exact numerical results. This agreement indicates that all assumptions/approximations used to derive Equation (15) are indeed justified. This allows us to address within the framework of the master equation the more complex problem, where the transport channel connects two high-temperature reservoirs with different filling factors.

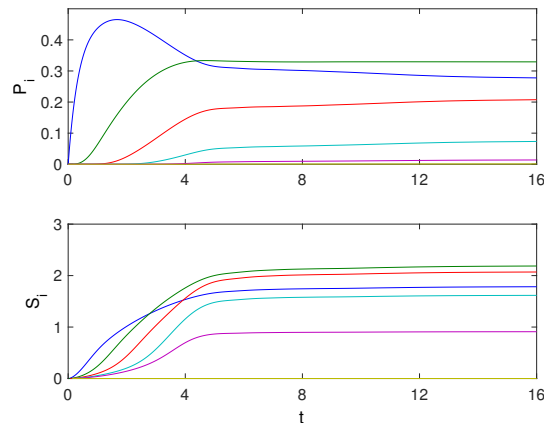


Figure 4. The same quantities as in Figure 2 yet calculated by using the master equation approach. The value of the relaxation constant is adjusted to $\gamma = 0.4$.

4.2. Stationary Current between Two Reservoirs

To take into account the second reservoir the master Equation (15) on the reduced density matrix should be complimented by two additional Lindblad terms which has the same structure as the Lindblad terms in Equation (15) but involves operators \hat{c}_L^\dagger and \hat{c}_L instead of the operators \hat{c}_1^\dagger and \hat{c}_1 . From this point we redefine the parameters \bar{n} and γ as \bar{n}_L and γ_L (the left reservoir). Correspondently, the filling factor and relaxation constant of the right reservoir are denoted by \bar{n}_R and γ_R and, to be certain, we assume $\bar{n}_L > \bar{n}_R$.

The solution of the described master equation with the source and sink terms was discussed in Reference [19] for the case of bosonic carriers. Adopting the results of Reference [19] to the present case of fermionic carries we come to the following conclusions. In course of time SPDM relaxes to the three-diagonal matrix where (pure imaginary) off-diagonal elements of the matrix determine the stationary current \bar{j} between the left and right reservoirs. This current is proportional to difference in the reservoir filling factors, where the proportionality coefficient A has particularly simple form in the case $\gamma_L = \gamma_R \equiv \gamma$,

$$A = \frac{1}{2} \frac{J\gamma}{J^2 + \gamma^2}, \tag{18}$$

and in the case $\gamma_R \ll \gamma_L \equiv \gamma$,

$$A = \frac{\gamma_R \gamma}{J^2 + \gamma^2}. \tag{19}$$

The latter case is of special interest for the purpose of microscopic analysis of the system dynamics. Indeed, if $\gamma_L \gg \gamma_R$ then the main source of decoherence is the left reservoir while the right reservoir barely serves as a particle sink. In the next subsection we analyze the problem where the left reservoir is modelled microscopically while the right reservoir is taken into account by using the master equation approach.

4.3. Quasi-Stationary Current

Following the discussion in the previous subsection, we consider the master equation

$$\begin{aligned} \frac{d\mathcal{R}}{dt} &= -i[\hat{H}, \mathcal{R}] - \mathcal{L}_{loss}(\mathcal{R}), \\ \mathcal{L}_{loss}(\mathcal{R}) &= \frac{\gamma_R}{2} (\hat{c}_L^\dagger \hat{c}_L \mathcal{R} - 2\hat{c}_L \mathcal{R} \hat{c}_L^\dagger + \mathcal{R} \hat{c}_L^\dagger \hat{c}_L), \end{aligned} \tag{20}$$

where \hat{H} is the Hamiltonian of the left reservoir with the attached transport channel. Due to large dimension of the Hamiltonian we solve Equation (20) by using the stochastic approach [32]. Specifically, we solve the Schrödinger equation of the form [35]

$$d|\Psi\rangle = \left(-i\hat{H}dt - \frac{\gamma_R}{2}\hat{c}_L^\dagger\hat{c}_L dt + \sqrt{\gamma_R}\hat{c}_L d\zeta\right)|\Psi\rangle, \tag{21}$$

where $d\zeta$ is the Wiener process with $\overline{d\zeta} = 0$ and $\overline{d\zeta^2} = dt$. Within this approach the reduced density matrix $\mathcal{R}(t)$ is found by averaging the solution of Equation (21) over different realisations of the stochastic process, i.e., $\mathcal{R}(t) = \overline{|\Psi(t)\rangle\langle\Psi(t)|}$. The convergence of the averaging procedure is controlled against the condition $\text{Tr}[\mathcal{R}(t)] = 1$.

First we reproduce the result of Figure 3a. The lower solid line in Figure 5 shows the mean current in the transport channel for $\varepsilon = 0.1$ but slightly smaller system size $M = 10, L = 4$ (this reduces the dimension of the Hilbert space from $\mathcal{N} = 18,564$ to $\mathcal{N} = 3003$) and $\gamma_R = 0$. The exponential decay of the current is clearly seen. Next we set γ_R to a small value $\gamma_R = 0.04$. It is seen that $j(t)$ now decays to a finite value \bar{j} , i.e., we have a quasi-stationary current between the reservoirs. We stress that the observed rapid relaxation of the current to zero or finite value is exclusively due to decoherence effect of the left reservoir. In fact, matching the lower solid line to the solution of the master Equation (15) we find $\gamma_L = 0.24$. Thus we are indeed in the regime $\gamma_R \ll \gamma_L$ where one can neglect decoherence effect of the right reservoir.

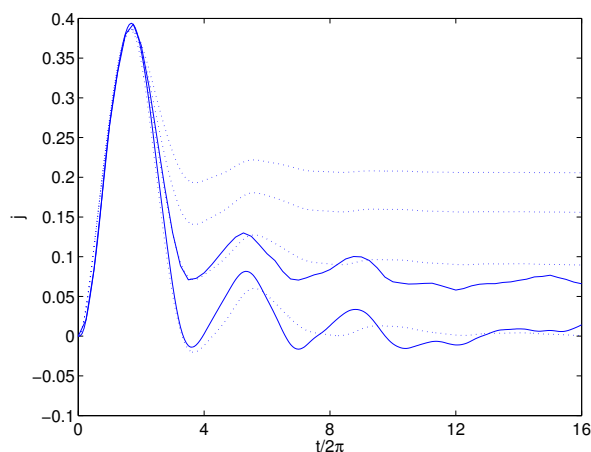


Figure 5. The mean current in the transport channel connecting two reservoirs. Dotted lines show solution of the master equation with the source ($\bar{n}_L = 0.5, \gamma_L = 0.24$) and sink ($\bar{n}_R = 0, \gamma_R = 0, 0.04, 0.08, 0.12$ from bottom to top) terms. The solid lines are solution of the master Equation (20) for $\gamma_R = 0$ and $\gamma_R = 0.04$.

5. Conclusions

We analyzed the quantum state of fermionic carriers in the transport channel connecting two reservoirs. The analysis is done from first principles by considering a microscopic model of the reservoir (Two-Body Random Interaction Model) and the transport channel (tight-binding chain of a finite length). In the case of infinite effective temperature of the reservoirs the single-particle density matrix (SPDM) of fermions in the channel is shown to relax to a three-diagonal matrix, whose off-diagonal elements determine the stationary current between the reservoirs. We stress that relaxation of SPDM to this steady state is entirely due to decoherence effect of the reservoirs on the carriers propagating in the channel. We obtain explicit expressions for the stationary current by justifying the master equation on the reduced density matrix of the carriers, which fortunately can be solved analytically. This first-principle justification of the master equation is one of the main results of the work.

The main challenge in the context of the presented studies is the case of low reservoir temperature, where occupation numbers of its natural orbitals show a step at the Fermi energy. It is believed that in this case the quantum state of fermionic carries in the transport channel is close to the Bloch wave with $k_F = \arccos[(\epsilon_F - V_g)/J]$. In the other words, the stationary SPDM has many non-zero diagonals. In principle, one can prove or disprove this conjecture numerically within the framework of the discussed microscopic model by considering a larger system size [that will reduce residual fluctuations in Figure 3b]. The other route is a generalization of the master Equation (15) onto the case of finite reservoir temperature, where it should include k_F as an additional parameter.

Author Contributions: Conceptualization, A.R.K.; investigation, A.R.K. and D.N.M.; writing—original draft preparation, A.R.K.; writing—review and editing, D.N.M.

Funding: This work has been supported by Russian Science Foundation through grant N19-12-0016. We appreciate discussion with Anna A. Bychek.

Conflicts of Interest: The authors declare no conflict of interest.

References

1. Datta, S. *Electronic Transport in Mesoscopic Systems*; Cambridge University Press: Cambridge, UK, 1997.
2. Ferry, D.; Goodnick, S.M. *Transport in Nanostructures*; Cambridge University Press: Cambridge, UK, 1999.
3. Ihn, T. *Semiconductor Nanostructures: Quantum States and Electronic Transport*; Oxford University Press: Oxford, UK, 2010.
4. Brantut, J.P.; Meineke, J.; Stadler, D.; Krinner, S.; Esslinger, T. Conduction of Ultracold Fermions Through a Mesoscopic Channel. *Science* **2012**, *337*, 1069–1071, doi:10.1126/science.1223175. [[CrossRef](#)] [[PubMed](#)]
5. Husmann, D.; Uchino, S.; Krinner, S.; Lebrat, M.; Giamarchi, T.; Esslinger, T.; Brantut, J.P. Connecting strongly correlated superfluids by a quantum point contact. *Science* **2015**, *350*, 1498–1501, doi:10.1126/science.aac9584. [[CrossRef](#)] [[PubMed](#)]
6. Krinner, S.; Stadler, D.; Husmann, D.; Brantut, J.P.; Esslinger, T. Observation of quantized conductance in neutral matter. *Nature* **2015**, *517*, 64–67, doi:10.1038/nature14049. [[CrossRef](#)] [[PubMed](#)]
7. Krinner, S.; Esslinger, T.; Brantut, J.P. Two-terminal transport measurements with cold atoms. *J. Phys. Condens. Matter* **2017**, *29*, 343003, doi:10.1088/1361-648x/aa74a1. [[CrossRef](#)]
8. Bruderer, M.; Belzig, W. Mesoscopic transport of fermions through an engineered optical lattice connecting two reservoirs. *Phys. Rev. A* **2012**, *85*, 013623, doi:10.1103/physreva.85.013623. [[CrossRef](#)]
9. Gutman, D.B.; Gefen, Y.; Mirlin, A.D. Cold bosons in the Landauer setup. *Phys. Rev. B* **2012**, *85*, 125102, doi:10.1103/physrevb.85.125102. [[CrossRef](#)]
10. Nietner, C.; Schaller, G.; Brandes, T. Transport with ultracold atoms at constant density. *Phys. Rev. A* **2014**, *89*, 013605, doi:10.1103/physreva.89.013605. [[CrossRef](#)]
11. Prosen, T. Exact Nonequilibrium Steady State of an Open Hubbard Chain. *Phys. Rev. Lett.* **2014**, *112*, 030603, doi:10.1103/physrevlett.112.030603. [[CrossRef](#)]
12. Simpson, D.; Gangardt, D.; Lerner, I.; Krüger, P. One-Dimensional Transport of Bosons between Weakly Linked Reservoirs. *Phys. Rev. Lett.* **2014**, *112*, 100601, doi:10.1103/physrevlett.112.100601. [[CrossRef](#)]
13. Chien, C.C.; Ventra, M.D.; Zwolak, M. Landauer, Kubo, and microcanonical approaches to quantum transport and noise: A comparison and implications for cold-atom dynamics. *Phys. Rev. A* **2014**, *90*, 023624, doi:10.1103/physreva.90.023624. [[CrossRef](#)]
14. Dujardin, J.; Argüelles, A.; Schlagheck, P. Elastic and inelastic transmission in guided atom lasers: A truncated Wigner approach. *Phys. Rev. A* **2015**, *91*, 033614, doi:10.1103/physreva.91.033614. [[CrossRef](#)]
15. Kordas, G.; Withaut, D.; Wimberger, S. Non-equilibrium dynamics in dissipative Bose-Hubbard chains. *Ann. Phys.* **2015**, *527*, 619–628, doi:10.1002/andp.201400189. [[CrossRef](#)]
16. Olsen, M.K.; Bradley, A.S. Quantum ultracold atomtronics. *Phys. Rev. A* **2015**, *91*, 043635, doi:10.1103/physreva.91.043635. [[CrossRef](#)]
17. Caliga, S.C.; Straatsma, C.J.E.; Zozulya, A.A.; Anderson, D.Z. Principles of an atomtronic transistor. *New J. Phys.* **2016**, *18*, 015012, doi:10.1088/1367-2630/18/1/015012. [[CrossRef](#)]

18. Lai, C.Y.; Chien, C.C. Challenges and constraints of dynamically emerged source and sink in atomtronic circuits: From closed-system to open-system approaches. *Sci. Rep.* **2016**, *6*, 37256, doi:10.1038/srep37256. [[CrossRef](#)] [[PubMed](#)]
19. Kolovsky, A.R.; Denis, Z.; Wimberger, S. Landauer-Büttiker equation for bosonic carriers. *Phys. Rev. A* **2018**, *98*, 043623, doi:10.1103/physreva.98.043623. [[CrossRef](#)]
20. Chakraborty, A.; Sensarma, R. Power-law tails and non-Markovian dynamics in open quantum systems: An exact solution from Keldysh field theory. *Phys. Rev. B* **2018**, *97*, 104306, doi:10.1103/physrevb.97.104306. [[CrossRef](#)]
21. Mintchev, M.; Santoni, L.; Sorba, P. Microscopic Features of Bosonic Quantum Transport and Entropy Production. *Ann. Phys.* **2018**, *530*, 1800170, doi:10.1002/andp.201800170. [[CrossRef](#)]
22. Sekera, T.; Bruder, C.; Belzig, W. Thermoelectricity in a junction between interacting cold atomic Fermi gases. *Phys. Rev. A* **2016**, *94*, 033618, doi:10.1103/physreva.94.033618. [[CrossRef](#)]
23. Bohigas, O.; Flores, J. Spacing and individual eigenvalue distributions of two-body random Hamiltonians. *Phys. Lett. B* **1971**, *35*, 383–386, doi:10.1016/0370-2693(71)90399-6. [[CrossRef](#)]
24. French, J.B.; Wong, S.S.M. Some random-matrix level and spacing distributions for fixed-particle-rank interactions. *Phys. Lett. B* **1971**, *35*, 5–7, doi:10.1016/0370-2693(71)90424-2. [[CrossRef](#)]
25. Flambaum, V.V.; Izrailev, F.M. Distribution of occupation numbers in finite Fermi systems and role of interaction in chaos and thermalization. *Phys. Rev. E* **1997**, *55*, R13–R16, doi:10.1103/physreve.55.r13. [[CrossRef](#)]
26. Kolovsky, A.R.; Shepelyansky, D.L. Dynamical thermalization in isolated quantum dots and black holes. *EPL (Europhys. Lett.)* **2017**, *117*, 10003, doi:10.1209/0295-5075/117/10003. [[CrossRef](#)]
27. Kolovsky, A.R.; Shepelyansky, D.L. Evaporative cooling and self-thermalization in an open system of interacting fermions. *arXiv* **2019**, arXiv:1902.06929.
28. Stöckmann, H.J. *Quantum Chaos: Introd*; Cambridge University Press: Cambridge, UK, 2007.
29. Haake, F. *Quantum Signatures of Chaos*; Springer: Berlin, Germany, 2010.
30. Åberg, S. Onset of chaos in rapidly rotating nuclei. *Phys. Rev. Lett.* **1990**, *64*, 3119–3122, doi:10.1103/physrevlett.64.3119. [[CrossRef](#)]
31. Breuer, H.P.; Petruccione, F. *Theory of Open Quantum Systems*; Oxford University Press: Oxford, UK, 2002.
32. Daley, A.J. Quantum trajectories and open many-body quantum systems. *Adv. Phys.* **2014**, *63*, 77–149, doi:10.1080/00018732.2014.933502. [[CrossRef](#)]
33. Kolovsky, A.R. Number of degrees of freedom for a thermostat. *Phys. Rev. E* **1994**, *50*, 3569–3576, doi:10.1103/physreve.50.3569. [[CrossRef](#)]
34. Kolovsky, A.R. Microscopic models of source and sink for atomtronics. *Phys. Rev. A* **2017**, *96*, 011601, doi:10.1103/physreva.96.011601. [[CrossRef](#)]
35. Goetsch, P.; Graham, R. Decoherence by spontaneous emission in atomic-momentum transfer experiments. *Phys. Rev. A* **1996**, *54*, 5345–5348, doi:10.1103/physreva.54.5345. [[CrossRef](#)]



© 2019 by the authors. Licensee MDPI, Basel, Switzerland. This article is an open access article distributed under the terms and conditions of the Creative Commons Attribution (CC BY) license (<http://creativecommons.org/licenses/by/4.0/>).